On Capturing Region-specific Effects of Traffic-state-dependent Trip Distances in Multi-region Bathtub Models

Jiayi Guo*[1], Irene Martínez[1], Gonçalo Correia[1], and Bart van Arem[1]

[1]Department of Transport & Planning, Faculty of Civil Engineering and Geosciences, Delft University of Technology, the Netherlands

Short summary

Multi-region bathtub models are widely applied to urban networks with unevenly distributed congestion. They require explicit modeling of regional path choice and flow exchanges. Regional paths are commonly defined as sets of routes that share the same sequence of traversed regions, and their distances can vary depending on traffic conditions. However, existing studies lack a systematic way to capture how regional traffic states affect path distances. This paper extends the multi-region bathtub model by incorporating dynamic path distance approximations for paths in each region. The extended model is evaluated on a partitioned road network of the city of Delft, the Netherlands. Bathtub model simulations with different path distance assumptions are benchmarked against a macroscopic traffic simulation. Results indicate that dynamic path distance approximation improves the accuracy of regional accumulation and speed in regions with large variations in path distance. In regions with limited path distance variation, static distances remain sufficient.
Keywords: Accumulation-based model, Macroscopic fundamental diagram, Multi-reservoir systems, Regional paths, Rerouting factor, Traffic-dependent trip distance

1 Introduction

Bathtub models have received increasing attention in research on urban traffic flow modeling and management (Johari et al., 2021). Bathtub models represent network-wide traffic dynamics by drawing an analogy between vehicle accumulation and water volume, and between traffic flow and water discharge. Traffic states are assumed to be homogeneous within an area, where the flow-density relationship can be represented by a Macroscopic Fundamental Diagram (MFD).

As the key relationship that describes traffic supply in bathtub models, the MFD has been validated against empirical data from cities with various topological structures (Geroliminis & Daganzo, 2008; Lu et al., 2018; Paipuri et al., 2020). However, increasing evidence indicates that MFDs are sensitive to spatial heterogeneity in demand distribution and congestion propagation, which can significantly affect network performance (Shim et al., 2019; Ambühl et al., 2021; Tilg et al., 2023). To capture the influence of traffic heterogeneity in the MFD, Knoop et al. (2015) introduced a generalized MFD that incorporates density and density deviation. Tilg et al. (2023) proposed a network method of cuts that considers the effect of demand patterns on MFD.

Rather than extending the MFD to account for heterogeneous areas, another widely used approach is to partition the network into regions with more homogeneous traffic states, thereby improving the validity of the homogeneity assumptions. Starting with Ji & Geroliminis (2012), many partitioning methods have been applied in bathtub models (Alayasreih et al., 2025). For multi-region bathtub models, components such as demand aggregation methods, flow exchange formulations, and merge rules have been investigated (Yildirimoglu & Geroliminis, 2014; Batista & Leclercq, 2019; Mariotte & Leclercq, 2019; Mariotte et al., 2020).

In addition to affecting the network supply, heterogeneous congestion also influences the demand through adaptive route choice behavior. Under heterogeneous congestion conditions, drivers may reroute to minimize travel time, which alters the effective trip distances. Batista et al. (2021) proposed an estimation method for traffic-dependent trip distances for inter-regional paths within

a regional dynamic traffic assignment (R-DTA) framework. Focusing on intra-regional rerouting, Guo et al. (2025) introduced a rerouting factor function (RFF) to approximate dynamic trip distances resulting from changes in congestion levels and demand distributions. In single-region settings, trip distance approximation has a relatively stable and direct influence on network dynamics, as the increment in trip distance leads to more severe congestion.

In contrast, it remains unclear whether intra-regional rerouting behavior significantly influences multi-region bathtub model dynamics. In a multi-region bathtub model, dynamic path distance approximations may also influence the flow exchange dynamics between regions, resulting in a more intricate impact on traffic states in all regions.

This paper investigates whether intra-regional RFF-based dynamic path distance approximations can improve the accuracy of a multi-region bathtub model. Specifically, we extend the multi-region accumulation-based bathtub model by incorporating a traffic-state-dependent rerouting factor function (RFF) to approximate dynamic path distances within regions using dynamic traffic states and aggregated network-demand properties. On a partitioned road network of the city of Delft, the Netherlands, the extended model is benchmarked against a macroscopic traffic simulation and bathtub simulations with static and dynamic path distance inputs.

2 Methodology

Multi-region bathtub model

This paper adopts the accumulation-based multi-region bathtub model proposed in (Mariotte & Leclercq, 2019; Mariotte et al., 2020). Assuming a negative exponential trip distance distribution, the accumulation-based bathtub model is formulated based on the conservation of vehicle accumulation in the network (Daganzo, 2007; Vickrey, 2020).

For multi-region cases, traffic dynamics are modeled at the regional path level, since vehicles on a path affect only the regions they traverse. Each path has a region sequence $S_p = (s_1, s_2, \ldots, s_{K_p})$, where s_K is the index of the Kth region traversed by path p and K_p is the total number of regions traversed by path p. For each region s, there is a set of internal paths $\mathcal{P}_s^{int}$ and a set of external paths $\mathcal{P}_s^{ext}$. Paths originating from the region are considered internal. Paths entering the region from outside are considered external.

Based on the accumulation-based model, the dynamics of path accumulation in region s are given by

$$\dot{n}_{p,s}(t) = q_{p,s}^{in}(t) - q_{p,s}^{out}(t) \tag{1}$$

where $n_{p,s(t)}$ denotes the accumulation of vehicles following path p in region s, $q_{p,s}^{in}(t)$ and $q_{p,s}^{out}(t)$ are the inflow and outflow of path p in region s at time t.

We describe the model using the flow evolution process illustrated in Figure 1. In the figure and the following description, the time index (t) for traffic states is omitted for clarity. For detailed formulations of the model, see Mariotte et al. (2020).

Consider a path p originating in Region 1 and ending in Region 2, traversing the macroscopic nodes m_1, m_2, and m_3, where C_m denotes the capacity of node m. As an internal path in Region 1, the inflow of p is not restricted and equals the path demand $\lambda_{p,1}$. At the boundary node m_2, the inflow of path p into Region 2 is equal to its outflow from Region 1, which is the minimum between the upstream outflow demand and the downstream inflow supply.

The outflow demand of path p in Region 1 $O_{p,1}$ is derived from the regional outflow demand function $P_1^g(n_1)$ (bottom-left plot). It is allocated to each path proportionally to its accumulation $n_{p,1}$. The downstream inflow supply for path p entering Region 2 $I_{p,2}$ is determined through a two-level merge process at node m_2 and at the regional boundary. Outflow demands of paths that enter Region 2 through m_2 are merged under the node capacity C_{m_2} using the Merge() algorithm (Leclercq & Becarie, 2012), resulting in node-level inflow supplies such as $I_{p,2}^*$.

For the second level, all paths entering Region 2 from upstream regions (i.e., all paths in $\mathcal{P}_2^{\text{ext}}$)

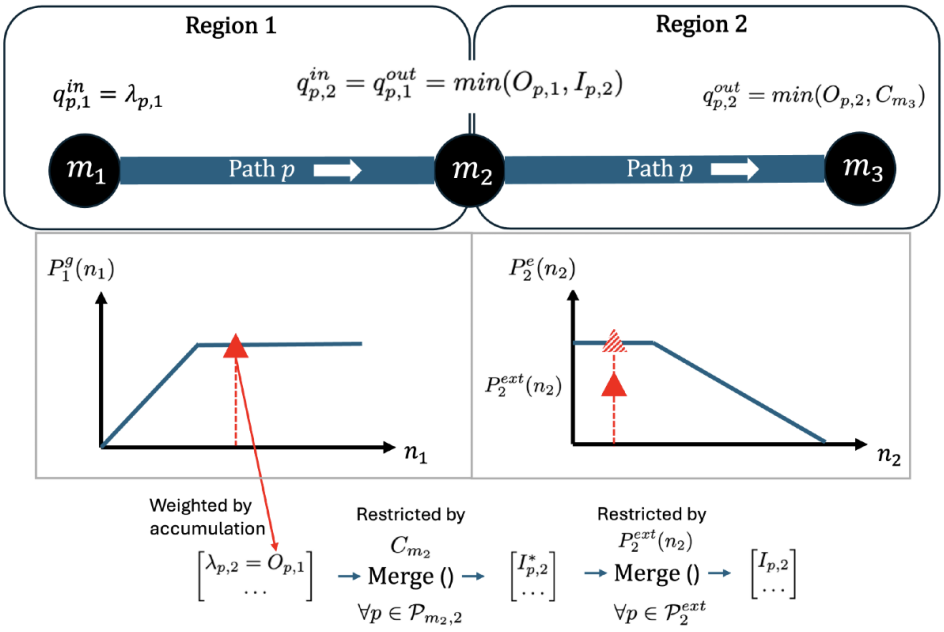


Figure 1: Conceptual illustration of flow evolution in the multi-region bathtub model

are jointly constrained by the receiving capacity of Region 2. The available capacity for external inflows is determined from the regional inflow supply function $P^e_2(n_2)$ (bottom-right plot), after prioritizing internal demand. Specifically, the effective capacity allocated to external paths is expressed as $P^{\text{ext}}_2(n_2) = P^e_2(n_2) - \sum_{p \in \mathcal{P}^{\text{int}}_2} \lambda_{p,2} D_{p,2}$, where $D_{p,2}$ is the distance of path p in Region 2. A second merge is then applied to paths in $\mathcal{P}^{\text{ext}}_2$, using $P^{\text{ext}}_2(n_2)$ as the capacity constraint, yielding the final inflow supplies $I_{p,2}$.

As path p terminates in Region 2, its outflow is determined by the minimum between its outflow demand $O_{p,2}$ and the capacity of the end node C_{m_3}. The end node capacity is typically assumed to be sufficiently large, ensuring that vehicles exiting the network are not constrained.

For the regional density-flow relationship, we use a smoothed trapezoidal MFD (Ambühl et al., 2020). The formulation gives an average outflow of region s

$$q_s(n_s(t)) = -h_s ln\left(exp\left(\frac{v^f_s n_s(t)}{h_s}\right) + exp\left(\frac{Q_s}{h_s}\right) + exp\left(\frac{-(\kappa_s - n_s(t))w_s}{h_s}\right)\right) \tag{2}$$

where $q_s(n_s(t))$ is the average outflow of region s at a density $n_s(t)$. h_s is a smooth parameter, v^f_s is the free-flow speed, Q_s is the average intersection capacity, κ_s is the jam density, and ω_s is the wave speed. In the accumulation-based model, the outflow expression can be converted into a production MFD with $P_s(n_s(t)) = q_s(n_s(t))L_s$, where L_s is the total length of the region in a unit of lane*km.

Rerouting factor function

To incorporate intra-regional rerouting effects into the multi-region bathtub model, we employ the rerouting factor function (RFF) (Guo et al., 2025). The RFF is defined as the ratio of the dynamic mean trip distance (MTD) to the shortest-path MTD for a region. For a single-region network, the RFF uses the OD matrix and route sets for each OD pair to calculate aggregated network-demand properties at each time step. In a multi-region network, the rerouting factor function for each region is defined as

$$\hat{\gamma}_s(v_s(t), \boldsymbol{\theta}_s) = \begin{cases} \gamma^f_s + \hat{a}_s \mu_s \left(1 - \dfrac{v_s(t)}{v^f_s}\right), & v_s(t) \geq v^{th}_s \\ \min\left(\hat{\gamma}_s(v^{th}_s, \boldsymbol{\theta}_s) + a_s p^{DRD}_s \left(\dfrac{v^{th}_s - v_s(t)}{v^f_s}\right)^{b_s}, 1 + c_s \bar{R}_s\right), & v_s(t) < v^{th}_s \end{cases} \tag{3}$$

where a_s, b_s, c_s, and $\hat{a}_s$ are scale parameters, and $v_s(t)$ is the average speed in region s. $\boldsymbol{\theta}_s(t)$ denotes the set of aggregated network-demand properties. It is defined as $\boldsymbol{\theta}_s = \{v_s^f, \gamma_s^f, \mu_s, v_s^{th}, p_s^{DRD}, \bar{R}_s\}$. As shown in Figure 2, each aggregated network-demand property determines a different component of the RFF curve.

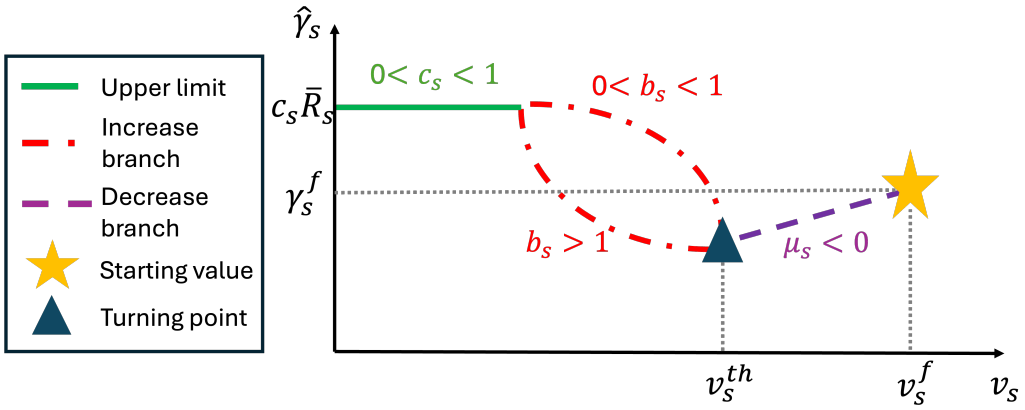


Figure 2: Conceptual illustration of the rerouting factor function

The free-flow speed v_s^f serves as a reference value for normalizing speeds across different networks. It is calculated as the average of free-flow speeds of routes weighted by their assigned demands. At v_s^f, the rerouting factor equals γ_s^f, which can be obtained from static traffic assignment results under free-flow conditions.

In regions where faster routes have longer distances, a two-branch RFF assumes a speed threshold v_s^{th} that separates the decrease and increase branches of $\hat{\gamma}$. The increasing and decreasing trends are defined relative to reductions in speed. The slope of the decrease branch is μ_s, and the slope of the increase branch depends on the proportion of route sets with large distance variation p_s^{DRD}. It is assumed that $\hat{\gamma}_s$ has an upper bound, affected by the average range of distances of route sets in the network $\bar{R}_s$. When the speed limit is uniform across the network, v_s^{th} coincides with v_s^f, and RFF reduces to a one-branch increasing trend, where Eq.3 is simplified with $v_s^{th} = v_s^f$, hence $\hat{\gamma}_s(v_s^{th}, \boldsymbol{\theta}_s) = \gamma_s^f$. The calculation of these aggregated network-demand properties is described in Guo et al. (2025).

Regional path aggregation and path attributes

In multi-region bathtub models, regional paths are defined using the macroscopic nodes in the network (as shown in Figure 1). The set of macroscopic nodes $\mathcal{M}$ includes all origin and destination centroids as well as transfer nodes (Mariotte et al., 2020). Each route r is associated with a sequence of nodes $\mathcal{M}_r = (m_1, m_2, \ldots, m_{K_r})$, where K_r denotes the total number of nodes traversed by route r. The route set corresponding to the regional path p is defined as $R_p := \{r \in \mathcal{R} \mid \mathcal{M}_r = \mathcal{M}_p\}$. where $\mathcal{R}$ is the full route set in the network. The demand on each regional path is

$$\lambda_p(t) = \sum_{r \in \mathcal{R}p} \lambda_{i_p j_p}(t) p_{i_p j_p r}(t) \tag{4}$$

where i_p and j_p are the origin and destination of regional path p, thus $i_p = \mathcal{M}_r[1], j_p = \mathcal{M}_r[K_r]$. $\lambda_{i_p j_p}(t)$ denotes the OD level demand at time t, and $p_{i_p j_p r}(t)$ represents the fraction of OD demand assigned to route r in dynamic traffic assignment.

Route distances are segmented according to the regions they traverse. In each region s, the segmented distance of route r is denoted as $d_{r,s}$. Using dynamic traffic assignment (DTA) results, the path distance of path p in region s is calculated as

$$D_{p,s}(t) = \frac{\sum_{r \in \mathcal{R}_p} d_{r,s} p_{i_p j_p r}(t)}{\sum_{r \in \mathcal{R}_p} p_{i_p j_p r}(t)} \tag{5}$$

Since $p_{i_p j_p r}(t)$ is affected by dynamic route choice behavior, the path distances (PD) are time- and traffic-state-dependent. Without the need to capture the route choice behavior in detail, the

RFF can be used to approximate the rerouting factor at the regional level. The approximated intra-regional rerouting factor is then applied to the path distances of all regional path segments within the region.

With macroscopic traffic simulation data, the dynamic PD $D_{p,s}(t)$ and free-flow PD $D^f_{p,s}$ are calculated as the weighted average over all route segments in the path, with demand on routes as the weight.

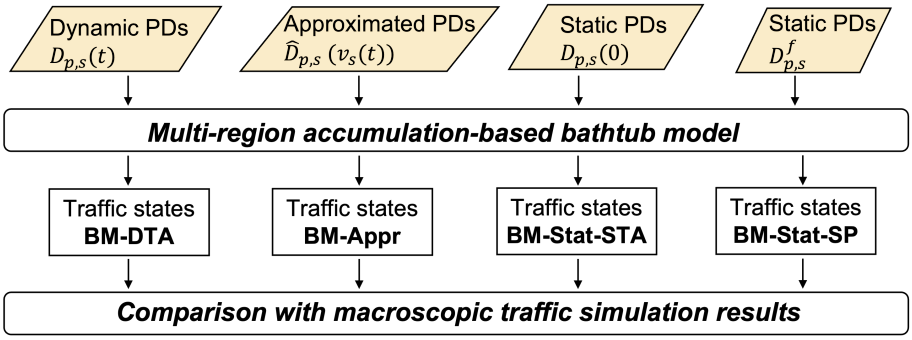


Figure 3: Assessment framework for the performance of RFF-extended multi-region bathtub model

Figure 3 shows a framework to assess the performance of the RFF-extended multi-region bathtub model. We create four cases with different regional PD inputs, including dynamic PDs $D_s(t)$ from dynamic traffic assignment, approximated PDs $\hat{D}_{p,s}(v_s(t)) = D^f_{p,s}\hat{\gamma}(v_s(t), \boldsymbol{\theta_s}(t))$, initial PDs $D_{p,s}(0)$ from static traffic assignment, and theoretical shortest PDs $D^f_{p,s}$. In the following, we refer to the 4 cases as BM-DTA, BM-Appr, BM-Stat-STA, and Stat-SP(shortest-path), respectively. Regional accumulation and speed results from the four cases are benchmarked against macroscopic traffic simulation results. Through cross-case comparison of the errors, the performance of the RFF-extended model is assessed.

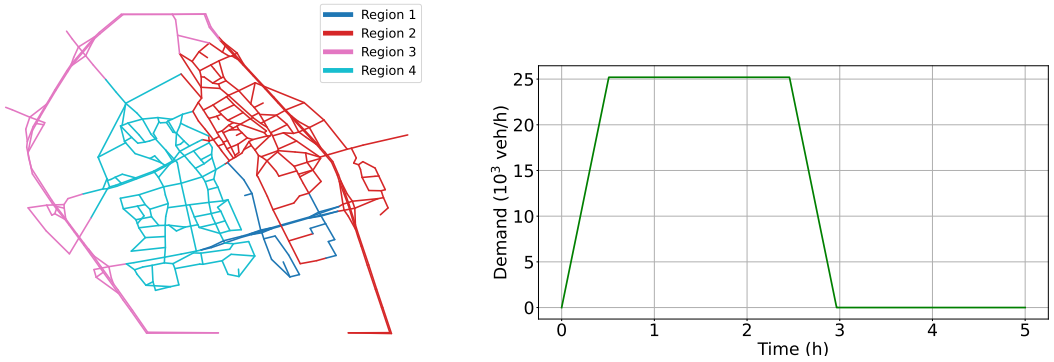
3 Results and discussion

For the comparative simulation analysis, we build bathtub model simulations for the road network of the city of Delft, the Netherlands. We use a macroscopic traffic simulation of Delft developed by DAT.Mobility (n.d.) as the benchmark. In the following, we refer to this simulation as the benchmark simulation.

As shown in Figure 4a, the network is partitioned into 4 regions based on the normalized cut (NCut) algorithm (Shi & Malik, 2000), with link density data from the benchmark simulation used as clustering features. Although Region 1 includes the most congested links, it cannot be separated directly by NCut under a four-region partition. To address this, we apply a heuristic procedure. First, the network is over-partitioned into a larger number of regions than required to ensure that the congested area corresponding to Region 1 is separated. After fixing Region 1, the remaining regions (2-4) are obtained by merging adjacent subregions based on spatial connectivity. The two north-south corridors located at the left and right edges of the network are two freeways.

The network is loaded with the demand profile shown in Figure 4b. We scale the demand profile using coefficients ranging from 0.45 to 0.47 to generate ten demand scenarios. Traffic state data from the benchmark simulation is aggregated at a one-minute resolution. The dynamic assignment is performed at 10-minute intervals, allowing congestion to evolve over time and influence subsequent pre-trip route choices. In the bathtub model simulations, a 30-second time step is used for traffic state and dynamic path distance updates. R-DTA is not implemented in the bathtub model simulations. We use the route-level DTA results from the benchmark simulation as dynamic path demand inputs (Eq.4).

All 64 border points created by the partitioning are retained as macroscopic nodes, resulting in a total of 87 macroscopic nodes (including 25 OD centroids). Based on these nodes, 4318 routes



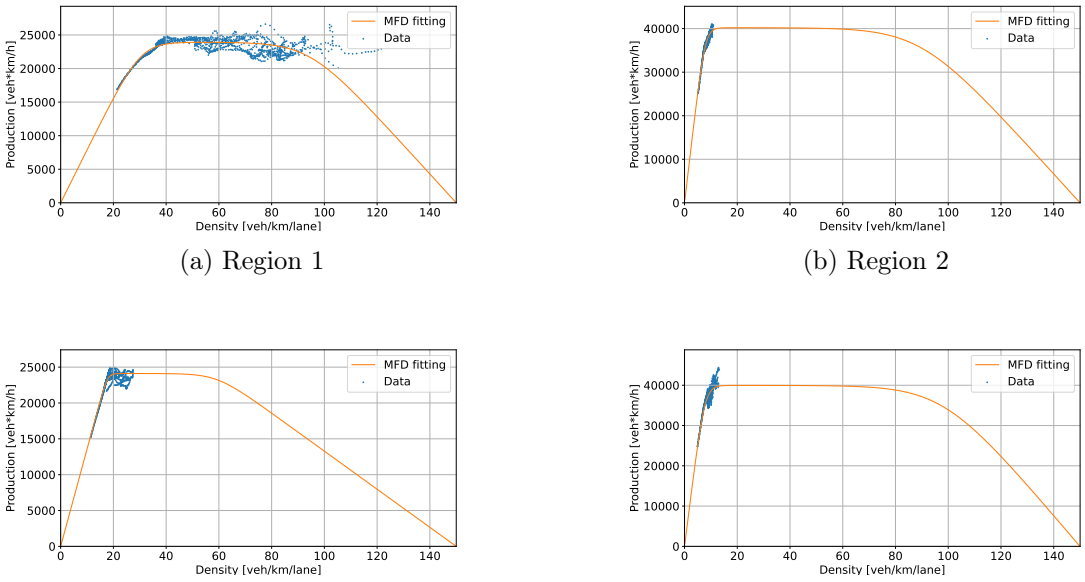
(a) Network structure and partition (b) Demand profile

Figure 4: Simulation network structure and demand profile

are aggregated into 1185 regional paths. Further aggregation of border nodes is possible, but it may amplify the impact of intra-regional rerouting, since the route set of each regional path becomes larger. Therefore, we begin with the least-aggregated regional path definition to exclude the influence of aggregation.

MFD and RFF calibration

Using density and speed data from the benchmark simulation, we calibrate the MFD for each region. The calibrated MFDs are shown in Figure 5. Region 1 is considerably more congested than Regions 2-4, underscoring the need for network partitioning in the Delft network. As there is a lack of congested observations, the jam density for Region 2-4 is fixed at 150 veh/km/lane.



(a) Region 1 (b) Region 2

(c) Region 3 (d) Region 4

Figure 5: MFD fitting results

We use the Genetic Algorithm to calibrate the RFF parameters. The calibrated regional RFFs are shown in Figure 6. For each region, the dots represent observed data (obs) and the crosses represent the RFF fits. In all four regions, the RFFs collapse to the one-branch form. It can be seen that RFF cannot capture γ_s for Regions 1 and 3. These two regions have very few route alternatives, thereby limiting the variation in MTD under congestion (as shown in Figure 4a). The high deviation of γ_3 around free-flow speed is because it has a highly uneven path distance distribution, a small change in demand fraction can lead to a drastic increase or decrease in γ_3

Table 1 lists the RFF parameter calibration results. nRMSE denotes the RMSE normalized by

the range (max–min) of observed values. For Regions 1 and 3, an R^2 value close to 0 indicates that the fitted curve describes the variation of data no better than the mean of the observations. Although RFFs for Regions 2 and 4 capture the increase of γ_s (as shown in Figure 6), the large gap between observed and fitted data at free-flow speed makes the nRMSE and R^2 of Region 2 the worst among the four regions. Data points where the ratio v_s/v_s^f exceeds 1 result from differences between the network demand distribution and the realized regional demand composition, as v_s^f is calculated with assigned demands as weights. For data points where $v_s/v_s^f \leq 1$, the nRMSE and R^2 are 0.221 and 0.093 for region 2, indicating that the fitted RFF captures some underlying MTD variation, although the overall explanatory power remains low.

Comparing the best-fit region with the single-region case (Guo et al., 2025), Region 4 has an R^2 higher than that of the single-region RFF, while its nRMSE is five times larger. In Figure 6, it can be seen that regional γ data are far more dispersed than network γ data. This indicates that RFF's performance is highly dependent on how paths are segmented. For better RFF fitting, the network may need to be partitioned using criteria beyond link density, such as the standard deviation and distribution type of the regional trip distance distributions.

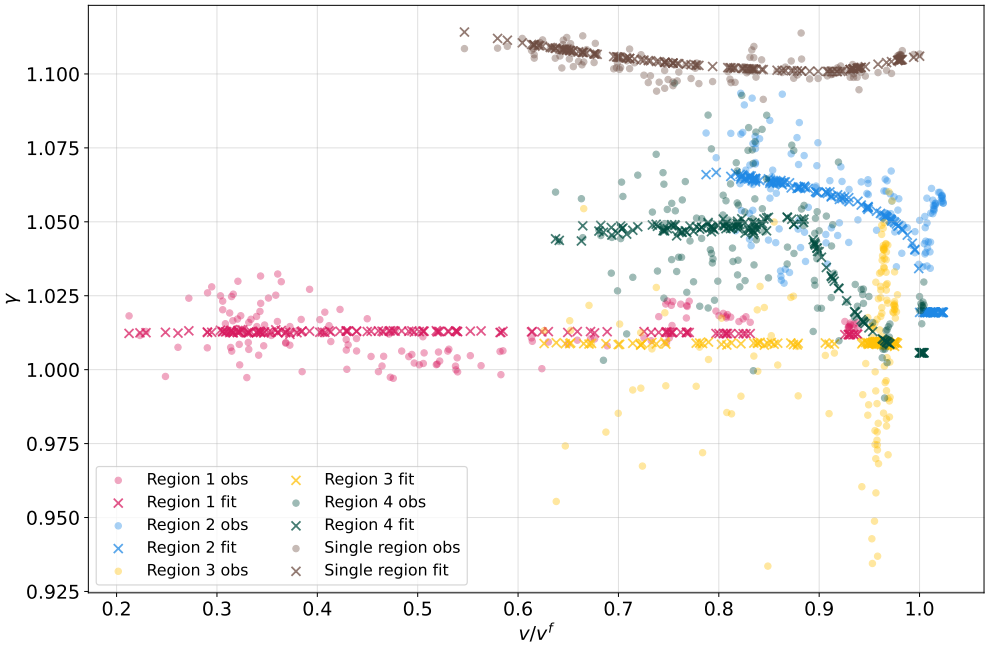


Figure 6: Rerouting factor function fitting results for the four regions and the single-region case

Table 1: RFF parameter calibration results

Calibration results	$\hat{a}$	a	b	c	nRMSE	R^2
Region 1	-	7.89	0.57	0.21	0.231	-0.025
Region 2	-	0.11	0.21	0.28	0.327	-1.331
Region 3	-	9.21	0.29	0.18	0.207	0.009
Region 4	-	7.34	2.05	0.13	0.161	0.362
Single region	0.1	0.06	1.90	0.39	0.034	0.247

Simulation results

For each demand scenario, we run bathtub model simulations for the BM-DTA, BM-Appr, BM-Stat-STA, and BM-Stat-SP cases. Focusing on the congestion-building period, we compare accumulation and speed results from 0.5 to 2.5 h with those from the benchmark simulation. The model performance during the congestion-resolving period is also influenced by whether hysteresis phenomena are included in MFD and RFF (Leclercq & Paipuri, 2019; Guo et al., 2025). Therefore,

modeling the congestion-resolving period is out of the scope of the present study.

Table 2 reports the mean errors normalized by the maximum accumulation or speed. Significance marks (*) indicate whether the mean error differs significantly from the BM-DTA case based on the independent-samples t-test. It can be seen that the results in the BM-Stat-SP case are relatively far from those of the other cases across all regions, indicating that static path distances should not be derived from minimum path distances. For Regions 1 and 3, limited path distance variations lead to close performance in the BM-DTA and BM-Stat-STA cases. For these two regions, applying the approximation method cannot improve the accuracy of the model. Regions 2 and 4 both show improvement in the BM-Appr case. For Region 2, BM-Appr has errors closer to BM-DTA than BM-Stat-STA. For Region 4, BM-Appr outperforms both BM-DTA and BM-Stat-STA. Figure 7 shows the accumulation and speed curves of the four regions in one demand scenario, illustrating the differences across the scenarios more directly.

Table 2: Normalized mean errors of bathtub model simulations in all regions

Variable	**Region**	**Normalized mean error**			
		BM -DTA	**BM -Appr**	**BM -Stat-STA**	**BM -Stat-SP**
Accumulation	**Region 1**	0.003	-0.006**	0.004	-0.020***
	Region 2	-0.027	-0.031	-0.040***	-0.114***
	Region 3	0.031	0.036	0.030	0.025*
	Region 4	-0.045	-0.028**	-0.046	-0.110***
	Single region	0.072	0.112***	0.069	-
Speed	**Region 1**	-0.005	0.001**	-0.006	0.015***
	Region 2	0.037	0.037	0.045**	0.088***
	Region 3	-0.018	-0.019	-0.018	-0.017
	Region 4	0.032	0.019**	0.033	0.081***
	Single region	-0.096	-0.133***	-0.023***	-

Note: * $p < 0.05$, ** $p < 0.01$, *** $p < 0.001$.

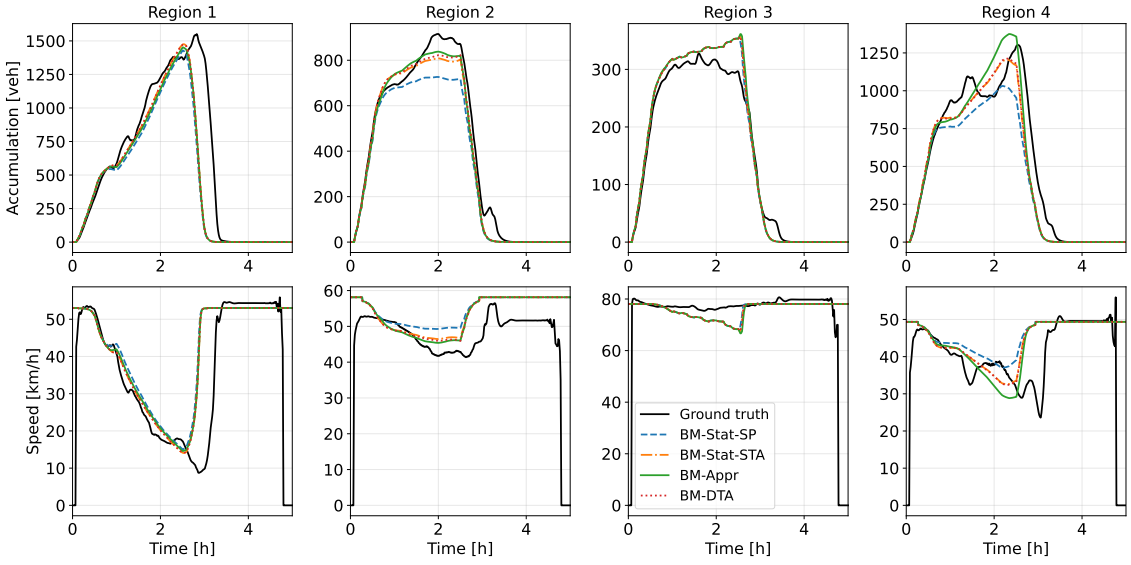


Figure 7: Simulation results from the scenario with demand coefficient of 0.456

Compared with the single-region bathtub model, multi-region bathtub models generally have lower errors. As for the performance of the RFF-extended model, the multi-region case shows clear and consistent improvement on both speed and accumulation accuracy in Regions 2 and 4. The BM-Appr case has a closer mean error to the BM-DTA case in Region 2 and the smallest error among all cases in Region 4. This suggests that partitioning not only improves regional homogeneity but also isolates regions where dynamic path distance has a stronger impact, allowing its influence to be captured more accurately at the regional level.

4 Conclusions

In this paper, we extend a dynamic mean trip distance approximation method (i.e., rerouting factor function) to regional paths in a multi-region setting and conduct a case study on the road network of Delft. We apply a partitioning method based on NCut and process regional benchmark data from macroscopic traffic simulations. By retaining all border transfer nodes, we define regional paths at a low level of aggregation. Through bathtub simulations with four path distance inputs, we observe improved accuracy in both accumulation and speed in two of the four regions, outperforming the single-region RFF-extend model.

We conclude that the influence of dynamic regional path distance varies across regions and is affected by the partitioning schemes. The path distance approximation method may not be necessary for all regions in a multi-region bathtub model, since regions with limited route alternatives exhibit small variation in path distance. In this study, the multi-region bathtub models rely on dynamic traffic assignment outputs for dynamic path demand. In future work, we will incorporate regional dynamic traffic assignment into the models and investigate how dynamic regional path distance approximations influence regional route choices across different levels of path aggregation.

References

Alayasreih, Y., Tilg, G., Dandl, F., Keyvan-Ekbatani, M., & Bogenberger, K. (2025). Cross-comparison of network clustering methods: potential Macroscopic Fundamental Diagram (MFD)-based applications. *Transportation Research Record Journal of the Transportation Research Board*, *2679*(12), 514–532. Retrieved from `https://doi.org/10.1177/03611981251353185` doi: 10.1177/03611981251353185

Ambühl, L., Loder, A., Bliemer, M. C., Menendez, M., & Axhausen, K. W. (2020). A functional form with a physical meaning for the macroscopic fundamental diagram. *Transportation research. Part B, Methodological*, *137*, 119–132. Retrieved from `https://doi.org/10.1016/j.trb.2018.10.013` doi: 10.1016/j.trb.2018.10.013

Ambühl, L., Loder, A., Leclercq, L., & Menendez, M. (2021). Disentangling the city traffic rhythms: A longitudinal analysis of MFD patterns over a year. *Transportation research. Part C, Emerging technologies*, *126*, 103065. Retrieved from `https://www.sciencedirect.com/science/article/pii/S0968090X21000917` doi: 10.1016/j.trc.2021.103065

Batista, S. F. A., & Leclercq, L. (2019). Regional dynamic traffic assignment framework for macroscopic fundamental diagram multi-regions models. *Transportation Science*, *53*, 1563-1590. doi: 10.1287/trsc.2019.0921

Batista, S. F. A., Leclercq, L., & Menéndez, M. (2021). Dynamic traffic assignment for regional networks with traffic-dependent trip lengths and regional paths. *Transportation Research Part C: Emerging Technologies*, *127*. doi: 10.1016/j.trc.2021.103076

Daganzo, C. F. (2007). Urban gridlock: Macroscopic modeling and mitigation approaches. *Transportation Research Part B: Methodological*, *41*, 49-62. Retrieved from `https://linkinghub.elsevier.com/retrieve/pii/S0191261506000282` doi: 10.1016/j.trb.2006.03.001

DAT.Mobility. (n.d.). *DAT.Mobility: data and it solutions in the field of mobility.* `https://www.goudappel.nl/en/dat-mobility`. (Accessed: 2025-08-19)

Geroliminis, N., & Daganzo, C. F. (2008). Existence of urban-scale macroscopic fundamental diagrams: Some experimental findings. *Transportation Research Part B: Methodological*, *42*, 759-770. doi: 10.1016/j.trb.2008.02.002

Guo, J., Martínez, I., Correia, G., & van Arem, B. (2025). On capturing dynamic trip distances in the bathtub model with a rerouting factor function. *Available at SSRN 5936873*.

Ji, Y., & Geroliminis, N. (2012). On the spatial partitioning of urban transportation networks. *Transportation Research Part B: Methodological*, *46*, 1639-1656. Retrieved from `https://linkinghub.elsevier.com/retrieve/pii/S0191261512001099` doi: 10.1016/j.trb.2012.08.005

Johari, M., Keyvan-Ekbatani, M., Leclercq, L., Ngoduy, D., & Mahmassani, H. S. (2021). Macroscopic network-level traffic models: Bridging fifty years of development toward the next era. *Transportation Research Part C: Emerging Technologies*, *131*, 103334. Retrieved from https://linkinghub.elsevier.com/retrieve/pii/S0968090X21003375 doi: 10.1016/j.trc.2021.103334

Knoop, V. L., Van Lint, H., & Hoogendoorn, S. P. (2015). Traffic dynamics: Its impact on the Macroscopic Fundamental Diagram. *Physica A Statistical Mechanics and its Applications*, *438*, 236–250. Retrieved from https://doi.org/10.1016/j.physa.2015.06.016 doi: 10.1016/j.physa.2015.06.016

Leclercq, L., & Becarie, C. (2012). MESO Lighthill-Whitham and Richards model designed for network applications. *Transportation Research Board 91st Annual MeetingTransportation Research Board*. Retrieved from https://trid.trb.org/view/1128675

Leclercq, L., & Paipuri, M. (2019). Macroscopic traffic dynamics under Fast-Varying demand. *Transportation Science*, *53*(6), 1526–1545. Retrieved from https://doi.org/10.1287/trsc.2019.0908 doi: 10.1287/trsc.2019.0908

Lu, S., Knoop, V. L., & Keyvan-Ekbatani, M. (2018). Using taxi GPS data for macroscopic traffic monitoring in large scale urban networks: calibration and MFD derivation. *Transportation research procedia*, *34*, 243–250. Retrieved from https://www.sciencedirect.com/science/article/pii/S2352146518303272 doi: 10.1016/j.trpro.2018.11.038

Mariotte, G., & Leclercq, L. (2019). Flow exchanges in multi-reservoir systems with spillbacks. *Transportation Research Part B: Methodological*, *122*, 327-349. Retrieved from https://linkinghub.elsevier.com/retrieve/pii/S019126151731175X doi: 10.1016/j.trb.2019.02.014

Mariotte, G., Leclercq, L., Batista, S., Krug, J., & Paipuri, M. (2020). Calibration and validation of multi-reservoir MFD models: A case study in Lyon. *Transportation Research Part B Methodological*, *136*, 62–86. Retrieved from https://doi.org/10.1016/j.trb.2020.03.006 doi: 10.1016/j.trb.2020.03.006

Paipuri, M., Xu, Y., González, M. C., & Leclercq, L. (2020). Estimating mfds, trip lengths and path flow distributions in a multi-region setting using mobile phone data. *Transportation Research Part C: Emerging Technologies*, *118*. doi: 10.1016/J.TRC.2020.102709

Shi, J., & Malik, J. (2000). Normalized cuts and image segmentation. *IEEE Transactions on Pattern Analysis and Machine Intelligence*, *22*(8), 888-905. doi: 10.1109/34.868688

Shim, J., Yeo, J., Lee, S., Hamdar, S. H., & Jang, K. (2019). Empirical evaluation of influential factors on bifurcation in macroscopic fundamental diagrams. *Transportation Research Part C: Emerging Technologies*, *102*, 509-520. doi: 10.1016/j.trc.2019.03.005

Tilg, G., Ambühl, L., Batista, S. F. A., Menéndez, M., Leclercq, L., & Busch, F. (2023). From Corridor to Network Macroscopic Fundamental Diagrams: A Semi-Analytical Approximation Approach. *Transportation Science*, *57*(5), 1115–1133. Retrieved from https://doi.org/10.1287/trsc.2022.0402 doi: 10.1287/trsc.2022.0402

Vickrey, W. (2020). Congestion in midtown manhattan in relation to marginal cost pricing. *Economics of Transportation*, *21*, 100152. doi: 10.1016/J.ECOTRA.2019.100152

Yildirimoglu, M., & Geroliminis, N. (2014). Approximating dynamic equilibrium conditions with macroscopic fundamental diagrams. *Transportation Research Part B Methodological*, *70*, 186–200. Retrieved from https://doi.org/10.1016/j.trb.2014.09.002 doi: 10.1016/j.trb.2014.09.002